Journal of Cerebral Blood Flow & Metabolism (2013) 33, 798–808

www.jcbfm.com

FEATURE ARTICLE

Chronic imaging of cortical blood flow using Multi-Exposure Speckle Imaging

Syed Mohammad Shams Kazmi[1], Ashwin B Parthasarthy[2], Nelly E Song[3], Theresa A Jones[4] and Andrew K Dunn[1]

Chronic imaging of cerebral blood flow (CBF) is an important tool for investigating vascular remodeling after injury such as stroke. Although techniques such as Laser Speckle Contrast Imaging (LSCI) have emerged as valuable tools for imaging CBF in acute experiments, their utility for chronic measurements or cross-animal comparisons has been limited. Recently, an extension to LSCI called Multi-Exposure Speckle Imaging (MESI) was introduced that increases the quantitative accuracy of CBF images. In this paper, we show that estimates of chronic blood flow are better with MESI than with traditional LSCI. We evaluate the accuracy of the MESI flow estimates using red blood cell (RBC) photographic tracking as an absolute flow calibration in mice over several days. The flow measures computed using the MESI and LSCI techniques were found to be on average 10% and 24% deviant ($n = 9$ mice), respectively, compared with RBC velocity changes. We also map CBF dynamics after photo-thrombosis of selected cortical microvasculature. Correlations of flow dynamics with RBC tracking were closer with MESI ($r = 0.88$) than with LSCI ($r = 0.65$) up to 2 weeks from baseline. With the increased quantitative accuracy, MESI can provide a platform for studying the efficacy of stroke therapies aimed at flow restoration.

Journal of Cerebral Blood Flow & Metabolism (2013) **33,** 798–808; doi:10.1038/jcbfm.2013.57; published online 10 April 2013

Keywords: chronic stroke imaging; Multi-Exposure Speckle Imaging; Laser Speckle Contrast Imaging; Laser Speckle Flowmetry

INTRODUCTION

Microcirculatory flows are increasingly becoming important as indicators of tissue health, particularly after an ischemic stroke.[1] Spatially resolved cerebral blood flow (CBF) dynamics can be used to gauge the severity of the infarct for potential neuronal viability, especially in the critical penumbra region. Beyond acute therapies administered early on stroke onset, primarily in the form of thrombolytics, the notion of a chronic period of residual neuroplasticity is also actively being investigated in rodents.[2–4] The residual perfusion levels in the affected areas likely have a significant role in the degree of neural and vascular remodeling. Therefore, there is a need for a relatively noninvasive and quantitative assessment of CBF over functionally sized regions of the cortex down to the level of the microcirculation that can be performed repeatedly in the same animal over a period of weeks to months.

In rodents, optical techniques for imaging flow are either based on tracking erythrocytes in space and time or from dynamic light scattering. Examples of the former include laser scanning microscopy,[5,6] as well as high-frame rate red blood cell (RBC) photography,[7,8] while the latter include Laser Doppler Flowmetry[9,10] and Laser Speckle Contrast Imaging (LSCI). Among these techniques, LSCI has recently emerged as the tool to use in rodent cortical blood flow imaging but has been largely limited to acute studies of neurovascular disease models[11–15] and functional activation.[16–18] Stroke studies in particular benefit from the intrinsic contrast obtained from imaging the effects of dynamic light scattering without introducing exogenous contrast agents into the bloodstream.[19] These studies range from providing a largely qualitative perspective of the presence or absence of flow[20] to the use of dynamic light scattering models to register a quantitative measure of CBF dynamics.[21]

The flow estimates from traditional single-exposure LSCI are relative and sensitive to a number of nonflow related parameters, which affect the ability to establish a quantitative baseline.[13,22] Recently, an extension to LSCI called Multi-Exposure Speckle Imaging (MESI) was introduced that improves the quantitative accuracy of the blood flow images.[23] The MESI technique uses an improved mathematical model and instrumentation to more precisely extract the flow-related contributions to the observed speckle contrast, as exhibited in controlled microfluidic flow phantoms[23] as well as *in vivo* rodent imaging. Particularly, measurements of acute flow changes during middle cerebral artery (MCA) occlusion[24] showed that single-exposure LSCI often underestimates large flow changes, while MESI accurately estimates the complete flow reductions. In this paper, we evaluate the accuracy and reproducibility of the MESI flow parameter by using high-frame rate RBC photography (e.g., RBC tracking) as an absolute flow calibration, while tracking chronic CBF changes in mice over several days.

MATERIALS AND METHODS

Animal Preparation

Mice (CD-1, male, 25 to 30 g, Charles River) were anesthetized with 70% N_2/O_2 vaporized isoflurane (2% to 3%) via a nose-cone. Temperature was maintained at 37°C with a feedback temperature control system (FHC Bowdoin, ME, USA) and arterial oxygen saturation was monitored via pulse

[1]Department of Biomedical Engineering, The University of Texas at Austin, Austin, Texas, USA; [2]Department of Physics and Astronomy, University of Pennsylvania, Philadelphia, Pennsylvania, USA; [3]The University of Texas Medical School at Houston, Houston, Texas, USA and [4]Department of Psychology, The University of Texas at Austin, Austin, Texas, USA. Correspondence: Dr AK Dunn, Department of Biomedical Engineering, The University of Texas at Austin, 107 West Dean Keeton C0800, Austin, TX 78712, USA.
E-mail: adunn@utexas.edu

This study was supported by the National Institutes of Health (EB011556), National Science Foundation (CBET/0737731) and the Coulter Foundation.
Received 2 January 2013; revised 28 February 2013; accepted 3 March 2013; published online 10 April 2013

oximetry (MouseOx; Starr Life Sciences Corp., Oakmont, PA, USA). Before sterile surgery, mice were administered carprofen (5 mg/kg, subcutaneous) and dexamethasone (2 mg/kg, intramuscular injection) to prevent inflammation after skull removal. Surgical instruments and artificial cerebral spinal fluid exposed to incision area were sterilized via autoclave. Mice were placed supine with the head affixed to a stereotaxic frame (Narshige, Narishige Scientific Instrument Lab, Tokyo, Japan). The scalp was shaved and resected to expose skull between bregma and lambda skull sutures. A 2- to 3-mm diameter portion of skull was removed with a dental drill (Ideal Microdrill, 0.8 mm burr; Fine Science Tools, Foster City, CA, USA) with constant artificial cerebral spinal fluid (buffered pH 7.4) perfusion. Cyanoacrylate (Vetbond, 3M, St. Paul, MN, USA) was added to exposed skull areas to facilitate dental cement adhesion. A 5- to 8-mm round coverglass (#1.5, World Precision Instruments, Sarasota, FL, USA) was placed on the brain with artificial cerebral spinal fluid perfusion between the exposed brain and the glass. Dental cement mixture was then wicked around the coverslip perimeter and sealed to the surrounding skull, while retaining gentle pressure on the coverslip to keep an air-tight seal for sterility and to restore intracranial pressure after craniotomy. A layer of cyanoacrylate was applied over the dental cement to fill porous regions and further seal the cranial window. Animals were allowed to recover from anesthesia and monitored for behavior normality before imaging.

Multi-Exposure Speckle Imaging of Blood Flow

Multi-Exposure Speckle Imaging was performed as described previously.[24] Briefly, a laser diode ($\lambda = 660$ nm, Micro Laser Systems, Garden Grove, CA, USA) illuminated the craniotomy via exposure and amplitude gating through an acousto-optic modulator, while simultaneously triggering 15 camera (A602f; Basler Vision Technologies, Ahrensburg, Germany) exposure durations spanning 4 decades (0.05 to 80 ms). Backscattered light was collected by a $\times 10$ objective (Figure 1) and imaged onto the camera. A 7×7 pixel window was used to convert the raw frames to speckle contrast images,[25] where speckle contrast is defined as the ratio of the standard deviation (σ_s) to the mean of the recorded intensity ($\langle I \rangle$) in the window:

$$K = \frac{\sigma_s}{\langle I \rangle} \tag{1}$$

The 15 single-exposure speckle images (Figure 2A) comprise one MESI computed frame (Figure 2B). The MESI model maps the dependence of the speckle contrast, K, on the exposure duration of the camera, T, (Figure 2C) to obtain an estimate of the correlation time of the speckles, τ_c:

$$K(T,\tau_c) = \left\{ \beta\rho^2 \frac{e^{-2x} - 1 + 2x}{2x^2} + 4\beta\rho(1-\rho)\frac{e^{-x} - 1 + x}{x^2} + v_{ne} + v_{noise} \right\}^{1/2} \tag{2}$$

where $x = \frac{DT}{\tau_c}$, ρ is the fraction of light dynamically scattered, β is a normalization factor to account for speckle sampling, v_{ne} is a nonergodic variance due to spatial (e.g., ensemble) sampling of temporal phenomena, and v_{noise} accounts for instrument noise.[23] Given simplifying assumptions based on laser Doppler flowmetry,[9] the inverse correlation time (ICT: $1/\tau_c$) has been posed to be proportional to the speed of the moving particles ($1/\tau_c \propto$ speed). A unitless weighting term, D, proportional to the vessel caliber is used to scale the correlation times inversely to account for the disparity in the number moving particles encountered between single vessels of differing sizes, as each scattering event off of a moving erythrocyte further decorrelates the speckles observed at the camera.[26–28] Contributions to speckles from parenchyma regions, however, cannot be decoupled or attributed to single vessels, and ICTs can rather be treated merely as a regional perfusion index[16,17,29] integrating scattering from a host of unresolvable depth-distributed microvasculature.

Traditional single-exposure LSCI measurements were extracted from the MESI acquisition by selecting the frames corresponding to the 1, 5, and 10 ms single exposures, respectively. These are the camera exposure durations most commonly used for *in vivo* studies[30] and have been shown to have optimal flow sensitivity in rodents.[31] Laser Speckle Contrast Imaging correlation times were calculated from the speckle contrast values using the expression[32]:

$$K(T,\tau_c) = \left(\beta \frac{e^{-2x} - 1 + 2x}{2x^2} \right)^{1/2} \tag{3}$$

Parameters in equation (3) retain the definitions and assumptions introduced in the MESI expression (equation 2). Comparisons between changes in ICT ($1/\tau_c$) dynamics herein are tested against centerline speed dynamics in single vessels garnered by RBC tracking from surface microvasculature within the field of view (FOV). Speckle region of interest (ROI) selection is placed well within the vessel lumen of the speckle images (Figures 2A and 2B), where the spatial flow profile appears shallow and thereby enables better correspondence to centerline flows.

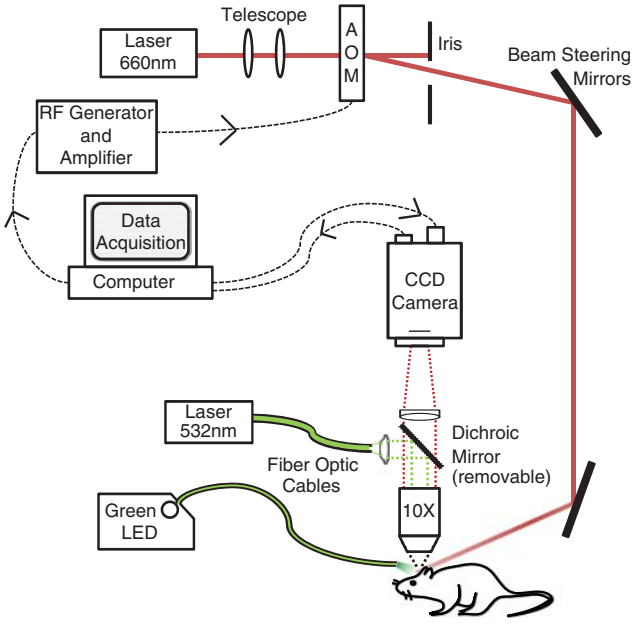

Figure 1. Schematic of combined multiexposure speckle and red blood cell (RBC) reflectance imaging. Pixel size in the object plane was 2.3 μm, which approximates to 3 pixels per erythrocyte. Dichroic mirror was introduced for conducting focused photo-thrombosis. AOM, acousto-optic modulator. CCD, charge coupled device; LED, light emitting diode; RF, radio frequency.

Red Blood Cell *Tracking*

A fiber coupled green LED (MSB-RGB, DiCon Lighting, Richmond, CA, USA) illuminated the craniotomy with oblique incidence. The mouse cortical surface was imaged using the same collection optics and camera (Figure 1) for speckle imaging but operated at 495 frames per second accomplished through ROI downsizing. Green light provides absorption contrast between hemoglobin in RBC's and blood plasma, which enables tracking of RBC movement in space and time (Figure 2D). Region of interest downsizing ($100 \times \sim 350$ pixels) was used to achieve the desired frame rates (495 frames/s) and therefore required multiple regional images to cover the entire FOV spanned during speckle imaging. A centerline section of a selected vessel was extracted from a set of repeating green reflectance images (see Supplementary Video) to track RBCs, which appear as negative contrast in a space-time composite, akin to a linescan (Figure 2D). A moving window and radon transform is used to determine the inclination of the streaks in the linescan from which average velocity estimates may be calculated[33] provided that the frame rate and spatial lengths are known. Spatio-temporal sampling of RBCs was optimized to obtain absolute velocities (Figure 2E) in selected vasculature with a maximum set uncertainty of 10% in the velocity estimates.[7]

Vascular Occlusions via Photo-Thrombosis

For occlusion studies, mice were administered with Rose Bengal (0.2 mL, 15 mg/mL, intraperitoneal), which has been shown to be fast-clearing photo-thrombotic agent.[20,34,35] A green laser (532 nm, Millenia V, Spectra Physics, Santa Clara, CA, USA) was fiber coupled into the objective system to deliver focused illumination (1.5 mW, source attenuated; Figure 1) over a targeted set of vasculature. Real-time LSCI was used to monitor the formation of the clot and control the duration of the photo-activation for the desired extent of occlusion. Postocclusion imaging began ~ 1 hour after photo-thrombosis to allow for Rose Bengal clearance from circulation.

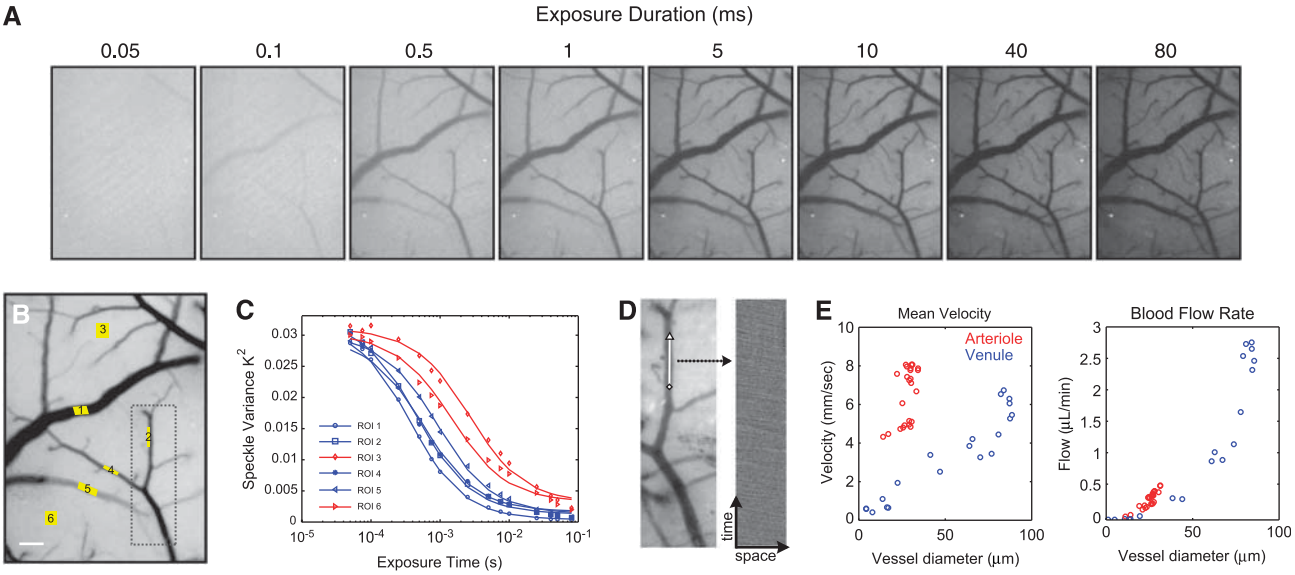

Figure 2. (**A**) Representative single-exposure speckle contrast images (15 exposures total, 8 shown). (**B**) Multi-Exposure Speckle Imaging Inverse Correlation Time (MESI ICT) image of flow computed from 15 exposures. Darker pixels are linearly representative of increasing flow. Scale bar = 150 μm. (**C**) MESI-computed speckle visibility curves for selected regions of interest (ROIs) in (**B**). Six ROIs selected for correlation time computation: four of which are centered in large surface vessels (blue curves) and two in areas without resolvable vasculature (red curves). (**D**) Green LED illuminated reflectance image (left) of cortex corresponding to boxed region in (**B**). Centerline (white, 100 μm) represents region over which red blood cells (RBCs) tracked. RBC time course (right) corresponding to selected vessel's centerline compiled from sequential images (see Supplementary Videos). (**E**) Extracted mean RBC velocity versus vessel diameter from RBC tracking and corresponding blood flow rate computed from centerline velocities and vessel cross-sections.

Experiment Protocol

Cranial window implanted mice were anesthetized and affixed to a stereotaxic frame, as described above, at least 1 day after surgery to reduce postsurgical physiologic instability unless otherwise indicated. Arterial oxygen saturation and heart rate from pulse oximetry were recorded and temperature was maintained via feedback as described earlier. Heart rate was matched within 10% between imaging sessions to guide physiologic control of cardiac output by controlling depth of anesthesia. First, speckle contrast imaging was performed by collecting 300 frames at each exposure. For ICT computations, 1/15 of the MESI sequences, uniformly distributed over the entire acquisition period (7.5 minutes), were averaged to hold the number of frames and thereby sampling periods constant between LSCI and MESI. Immediately after speckle imaging, RBC tracking over eight subregions of the FOV lasted $\sim$5 minutes. Over any given vessel of interest, speckle imaging and RBC tracking acquisitions, each with the aforementioned frame or FOV reductions, spanned a period of 30 to 40 seconds. All experiments were approved by the Institutional Animal Care and Use Committee (IACUC) at The University of Texas at Austin under guidelines and regulations consistent with the Guide for the Care and Use of Laboratory Animals, the Public Health Service Policy on Humane Care and Use of Laboratory Animals (PHS Policy) and the Animal Welfare Act and Animal Welfare Regulations.

RESULTS

Speckle contrast images at several exposure durations are presented in Figure 2A from one imaging session. Qualitatively, a relative sensitivity from fast to slow flows can be inferred with increasing exposure duration, as expected. The exposure dependence of the speckle variance averaged over six ROIs (Figure 2B) is presented in Figure 2C. The speckle ICTs are computed by fitting each curve to equation (2) and enable mapping of the flow dynamics by analyzing the characteristic shapes of these curves. It is important to note the inflections in the speckle variance curves, as multiexposure implementations with fewer exposures[36,37] congregated in one or two decades of exposure duration may insufficiently capture this relationship and thereby inaccurately sample the flow distributions present, especially after induced flow changes. A true MESI ICT image of flow is generated from the 15 single-exposure speckle images in Figure 2B. Compared with any one exposure (Figure 2A), the MESI ICT image scale provides a more linear, uniformly sensitive, and comprehensive depiction of the cortical perfusion. Vessel caliber (e.g., multiple scattering) deweighting was not applied *a priori* to the MESI ICT image given the pixel-by-pixel computation, but can be easily included when interpreting data between surface vessels.

Red blood cell velocity distributions from high-frame rate reflectance imaging (i.e., RBC Tracking) were in accordance with vascular RBC velocity distributions in the murine brain reported elsewhere.[38,39] The velocity distribution with vessel size (Figure 2E) reveals a wide spread at the most prevalent vessel diameters resulting from the relatively medial anatomical location of the craniotomy and therefore sampling of disparate branch orders of arterioles and venules. Assuming cylindrical vessel geometry,[40] blood flow rate can be approximated as the product of the centerline speed of the RBCs and the cross-sectional area of the vessel (Figure 2E), which slightly underestimates the actual flux. Corrective terms have been suggested but have a larger impact when the vessel calibers diverge substantially from RBC sizes,[40,41] usually well above the microvascular regime. Venule cross-sections are not accurately predictable with two-dimensional imaging, as only the major axis of the ovular vascular lumen is discernable. Therefore, venular flow (Figure 2E) may be overestimated by this geometric discrepancy.

Quantitative Baseline Cerebral Blood Flow Dynamics

Initially, we compare MESI- and LSCI-computed ICTs from ROIs spanning the FOV with relative changes in flow obtained from RBC tracking averaged over the same FOV. Multiple ROIs were selected from the speckle images (Figures 2A to 2C). To facilitate paired

Table 1. Total number of animals, imaging sessions, and ROIs used for cross-modality comparison. Number of Sessions excludes initial imaging day used for normalization

Number of paired comparisons		
Group	*Animal*	*Sessions (ROIs)*
Baseline Physiology	1	4 (4)
	2	4 (4)
	3	4 (4)
	4	4 (4)
	5	5 (4)
	6	4 (6)
Occlusion Dynamics	7	7 (5)
	8	6 (5)
	9	6 (6)

ROIs, regions of interest. Percent deviation (% Δ): number of comparisons = number of sessions × number of ROIs. Correlation coefficient (r): number of comparisons = number of ROIs.

RBC tracking, cross-modality comparisons were limited to resolvable vessels with sufficient nonoverlapping projections in both imaging techniques.

From the results of chronic baseline imaging of six animals over several imaging sessions (Table 1) spanning 6 to 14 days (Figure 3) significant differences between flow measures estimates using LSCI (1 and 5 ms exposure duration) and RBC tracking can be seen over time, while flow measures estimated using MESI and RBC tracking maintain greater concordance. The relative flow measures from each technique were obtained by normalizing to the first imaging session, akin to typical analyses of relative CBF dynamics[11,14] and to provide a normalization factor for comparison between imaging modalities. Specifically, the MESI ICTs remain within a 95% confidence interval across all ROIs with RBC tracking over the chronic period, while LSCI estimates exceed these bounds in nearly all animals (Figure 3A). The error bars represent the standard deviation in the flow measures versus baseline over the vessel containing ROIs and were omitted from the relative RBC speeds for visual clarity. The first imaging session for the fifth animal (Figure 3A) was conducted immediately after cranial window implantation. The large change in flow after the first imaging session in this animal is likely due to the lack of a recovery period after surgery, which makes physiologic control difficult to sustain. For this reason, all remaining quantitative baseline data presented follow at least 1 day after surgery, especially for the occlusion studies presented below. In summary, the ensemble CBF dynamics presented in Figure 3A suggest greater confidence in the changes in correlation times computed using MESI in a chronic setting versus from LSCI. It is likely that illumination and specimen variations over the chronic period contributed to the discrepancies in single-exposure LSCI flow estimates. However, the consistency of the MESI flow measures with RBC tracking necessitated further examination and quantification.

Paired Dynamics over the Field Of View (Multi-Exposure Speckle Imaging vs Laser Speckle Contrast Imaging)

Average percent deviation (Figure 3B) of speckle ICTs from RBC velocity dynamics were computed for both the MESI and LSCI (1, 5, and 10 ms) techniques per each animal. As in Figure 3A, these measurements were normalized to the first imaging session. Again, comparisons were restricted to relative changes from paired single vessel containing ROIs over the number of imaging sessions listed in Table 1. The average percent deviation metric is indicative of the absolute accuracy of flow estimates from each speckle technique when compared with the RBC speed dynamics. On average, all animal studies retain deviations at or under $10 \pm 3\%$ between MESI ICTs and speeds from RBC tracking (Figure 3B). Baseline physiology Animals 1 to 4 and 6 showed greater accuracy with the MESI technique versus all three LSCI exposures. Only the 1-ms exposure LSCI retained comparable deviation with MESI in Animal 5, while MESI outperformed the remaining two LSCI single exposures. Occlusion dynamics' animals (Animals 7 to 9; Figure 3B) retained lower levels of deviation than all LSCI single exposures. The studies also show the disparity in accuracy that exists within the three single-exposure durations commonly selected for LSCI and highlight the physiologic variability in the baseline flow distributions with exposure duration (Animals 1 to 6) let alone after induced flow changes (Animals 7 to 9). Over all animal studies (Table 1), the average LSCI deviations with RBC tracking are $24 \pm 10\%$, $23 \pm 6\%$, and $24 \pm 7\%$ for the 1, 5, and 10 ms exposure durations, respectively.

As a second performance metric, the average correlation coefficients between the speeds from RBC tracking and speckle ICTs were computed to examine the proportionality and trend over each chronic study (Figure 3B). On average, the flow estimates between RBC tracking and the MESI technique maintained high correlation coefficients ($r = 0.88$) across the nine animals over the chronic period. Of the LSCI flow estimates, the 5-ms exposure duration yielded better trends ($r = 0.65$), while the 1 and 10 ms closely follow with comparable proportionality ($r = 0.63$). Three of the LSCI studies (Animals 2, 3, and 4) suggest no reliable trend ($r < 0.50$) between the RBC speed and computed ICTs, combined with greater variability on an ROI by ROI basis than seen with MESI (see errorbars; Figure 3B). Linear regression over all ROIs and imaging sessions ($n = 201$ evaluation points) measured after the first imaging session from all animals (Figure 3C) provides a more holistic comparison between MESI and single-exposure LSCI flow estimates. Given the slope of the regression curves (a) and goodness of fits shown (R^2), both in terms of their closeness to unity, stronger linearity exists between MESI-computed relative ICT's ($a = 0.90$, $R^2 = 0.88$) and RBC speed changes than with 5-ms exposure LSCI ($a = 0.65$, $R^2 = 0.50$). Additionally, MESI more closely predicts complete flow reductions by a factor of nearly fivefold, particularly important for chronic stroke studies, as exhibited by the y intercept of the regression curves (MESI: $b = 0.05$, LSCI: $b = 0.24$).

Occlusion Studies in Detail

Chronic cerebral blood flow measurements of sustained occlusions. To examine the accuracy of blood flow estimates obtained by the MESI technique, we induced a flow change comparable to a localized ischemic infarct spanning the size of a functionally relevant region of the mouse cortex (Figure 4). The first three imaging sessions (Days 2 to 4) comprised the baseline phase, followed by photo-thrombosis centered over regions specified in Figure 4A. Thereafter, four imaging sessions were performed for postocclusion analysis, spanning one full week. Figures 4B and 4C highlight the postinfarct blood flow dynamics.

Relative to baseline, the MESI-computed ICT images (Figure 4B) depict a greater degree of ischemia than predicted by LSCI ICT maps over time. Estimates of blood flow changes obtained with the MESI technique in the occlusion animal retain consistency with those from RBC tracking both during baseline and postocclusion phases (Figure 4C). For simplicity, detailed LSCI comparisons are limited to the 5-ms exposure given the lower average deviation and higher correlation observed over all animals (Figure 3B). Estimates of blood flow changes obtained using LSCI were found to be deviant from RBC tracking estimates by 18% on average. Specifically, the LSCI estimates from a few ROIs had up to a 25% deviation during baseline on Day 3 (see errorbars; Figure 4C), followed by a significant underprediction of the peak flow reduction between Days 7 and 9 (Figure 4C).

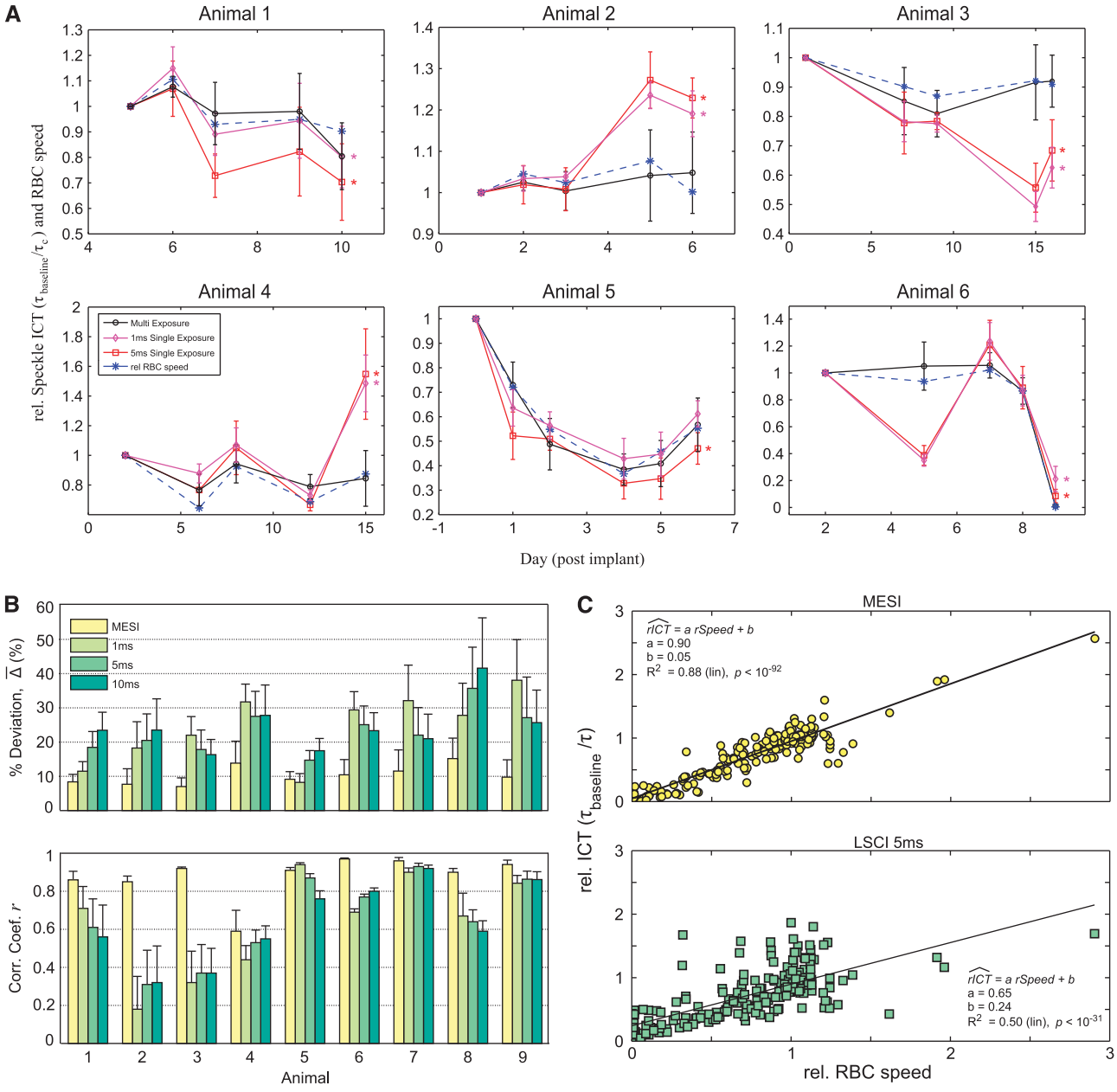

Figure 3. (**A**) Chronic baseline imaging of blood flow in six animals over varying durations. Relative inverse correlation times (ICTs) from Multi-Exposure Speckle Imaging (MESI) and Laser Speckle Contrast Imaging (LSCI) (1 and 5 ms exposures) are normalized to the first imaging session. Corresponding relative flow measures from red blood cell (RBC) tracking are included to register baseline flow dynamics with both speckle techniques. Data points and error bars represent avg ± s.d. over 4 to 6 vessels specifically enumerated in Table 1. Asterisk denotes statistically significant (*$P < 0.05$, repeated measures analysis of variance) difference between the LSCI and RBC tracking flow trends. Individual vessel and parenchyma flow trends are provided for some animals as Supplementary Information. (**B**) Average percent deviations ($\%\,\bar{\Delta}$) and average correlation coefficients (*r*) of chronic flow dynamics from MESI and LSCI (1, 5, and 10 ms exposures) against RBC speed changes within each animal. Data and error bars represent avg ± s.d. over number of regions of interest (ROIs) and imaging sessions specified in Table. (**C**) Linear regression of MESI and LSCI (5 ms) predicted flow dynamics versus those from RBC Tracking compiled from all comparison points ($n = 201$) across all animals.

In actuality, the average flow reduction in the large vessel containing ROIs was 90% and likely near 100% in areas without obvious surface vasculature (see parenchyma ROIs; Figure 4C). The expansion of the infarct in the days after photo-thrombosis can possibly be attributed to a substantial aggregation of thrombi at occlusion onset and subsequent clot dispersion, which can generate downstream occlusion and stenosis in the microvascular network over time. However by Day 12, flows in some of the selected vessels and underlying parenchyma slightly increase according to MESI, LSCI, and RBC tracking predictions (Figure 4C).

The results between MESI and LSCI (Figure 4) are similar to those measured acutely,[24] where single-exposure flow estimates underpredict the large-scale flow change from an MCA occlusion. Similarly, the flow measures averaged over all imaging session and ROIs (Figure 3B, Animal 7) depict lower deviation and higher correlations between MESI and RBC tracking than with the LSCI at 1, 5, and 10 ms exposures. Among the single-exposure LSCI measures, longer exposure durations yield better consistency with

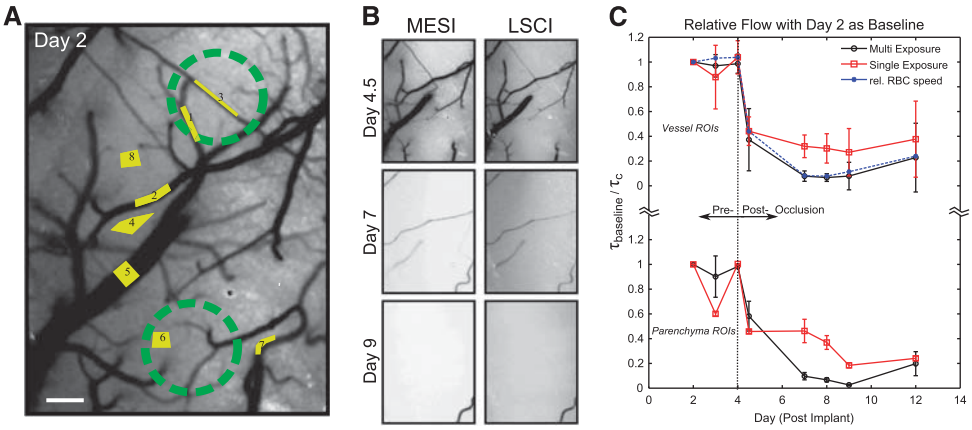

Figure 4. (**A**) Multi-Exposure Speckle Imaging inverse correlation time (MESI ICT) image of baseline flow. Labeled regions of interest (ROIs) correspond to both Laser Speckle Contrast Imaging (LSCI) and MESI computed flow indices averaged in (**C**). Areas selected for targeted photothromboses are marked with green circles. Scale bar = 150 μm. (**B**) MESI (left column) and 5 ms LSCI (right column) ICT image sequences after vascular occlusions. Day 4.5 imaging was conducted 1 to 2 hours after photo-thrombosis. (**C**) Average flow dynamics from MESI and LSCI versus red blood cell (RBC) tracking in large surface vessel containing regions (ROIs 1, 2, 3, 5, and 7) are presented. Additionally, parenchymal flow dynamics (ROIs 4, 6, and 8) are shown as well. Data points and error bars represent avg ± s.d. over five vessels and three parenchyma regions, respectively. No significant ($P > 0.05$, repeated measures analysis of variance) difference between speckle flow trends and RBC tracking over chronic period.

RBC tracking, likely due to the near-complete flow reduction for the majority of the imaging sessions. The MESI-computed ICT maps (Figure 4) present a chronic stream of images where the depicted perfusion exhibits the greatest confidence in accuracy and correlation with the actual flow dynamics present. Nonetheless, LSCI after typical frame averaging provided nearly real-time (10 Hz) pre and postocclusion perfusion monitoring. No significant differences in the average LSCI flow indices extracted from frames in the MESI acquisition and those obtained from continuous single-exposure imaging were observed while holding the total number of frames constant.

Transient occlusions: remodeling and redundancy. Single vessel occlusions can also be used to examine the sensitivity and specificity of the computed ICTs to varying regional flow changes. In one animal, a targeted occlusion (Figure 5) was performed of a branch of the anterior cerebral artery. Sustained collateral occlusions of two overlapping venules were also induced in the process. Inverse correlation time maps from LSCI and MESI overlay the speckle contrast images in Figure 5A to better highlight any regional discrepancy in the observed flow dynamics from each technique. These maps exhibit disparity in both the magnitude of the flow reduction and its spatial extent between the two speckle techniques. Specifically with flow under 15%, the area typically identified as the ischemic core is more readily discernable in both severity and expanse through the MESI predictions (Figure 5A, Day 5.5).

The observation of a residual flow level within 24 hours after occlusion along with a reversal in direction is also indicated in Figure 5A (see arrows). Due to the direction and latency of the observed collateral flow (Day 6, Figure 5A), there could be anastomoses[12] outside the observable FOV with arteriole branches of the MCA or a pure passive reversal of pressure gradients from existing collateral supply routes and drainage downstream of the targeted vessel.[42] Perfusion in the parenchyma branches remains reduced relative to baseline compared with large surface vasculature by Day 14. The MESI ICT maps also show greater recovery than the LSCI over the remaining period as well. On Day 6 and onwards (see boxed selections, Figure 5A), LSCI flow estimates also appear to register an errant 20% residual flow in a region due to a mixture of illumination, sample orientation, and static scattering artifacts, while MESI suggests a return to baseline levels of perfusion. By Day 14, flow does not restore in the venules that were occluded with the anterior cerebral artery; though recruitment of collateral drainage toward the region (see selection, Figure 5A) from the parent venule is now discernable. Overall, the underlying speckle contrast images highlight typical single-exposure LSCI artifacts and sensitivity inadequacy to flow distribution changes. However, the overlying MESI ICT maps appear less susceptible to such artifacts and ultimately may be more useful for identifying the ischemic core and penumbra accurately over a chronic period.

To validate the accuracy of the MESI ICT maps in Figure 5A, the relative MESI and LSCI ICTs are compared against the relative RBC speeds (Figures 5B and 5C). The MESI-computed ICT's retained lower average deviation ($\Delta = 15 \pm 5\%$) with RBC tracking and closer correlations ($r = 0.90 \pm 0.04$) than the three LSCI exposures (Animal 8, Figure 3). As the targeted occlusion largely affects one of the ROIs selected within the FOV, there exists greater spread in flow transients observed across the ROIs. We now examine each ROI independently in Figures 5B and 5C, where the main targeted arteriole is labeled as ROI 2.

Photo-thrombosis resulted in a transient flow reduction of several ROIs immediately after onset of the occlusion. One day after photo-thrombosis, the occlusion was retained only in the targeted vessel (ROI 2 in Figure 5B) and overlapping venules. The regional supply arteriole (ROI 1) branch of the anterior cerebral artery suffered only a 55% flow reduction, as estimated by RBC tracking. Both MESI and LSCI computed flow decrements immediately after occlusion agree well with RBC tracking. Additionally, ROIs 6 and 7 suggest a 60% flow reduction in the underlying and neighboring parenchyma. However, chronic postocclusion dynamics predicted by LSCI deviate substantially from RBC tracking over the selected ROIs. Collateral supply to the arteriole branch (ROI 4) was observed to restore flow to nearly 44% of baseline coupled with a transient blood flow reversal observed by RBC tracking (arrows, Figure 5A). A sustained flow increase in the large neighboring venule (ROI 5) was also observed but is likely associated with flow redistributions occurring beyond the FOV. After 1.5 weeks, arteriolar RBC speeds returned to 66% of baseline, as predicted by MESI and RBC tracking.

Core and peri-infarct dynamics. A larger FOV was used to examine penumbral remodeling after a targeted occlusion over a branch of

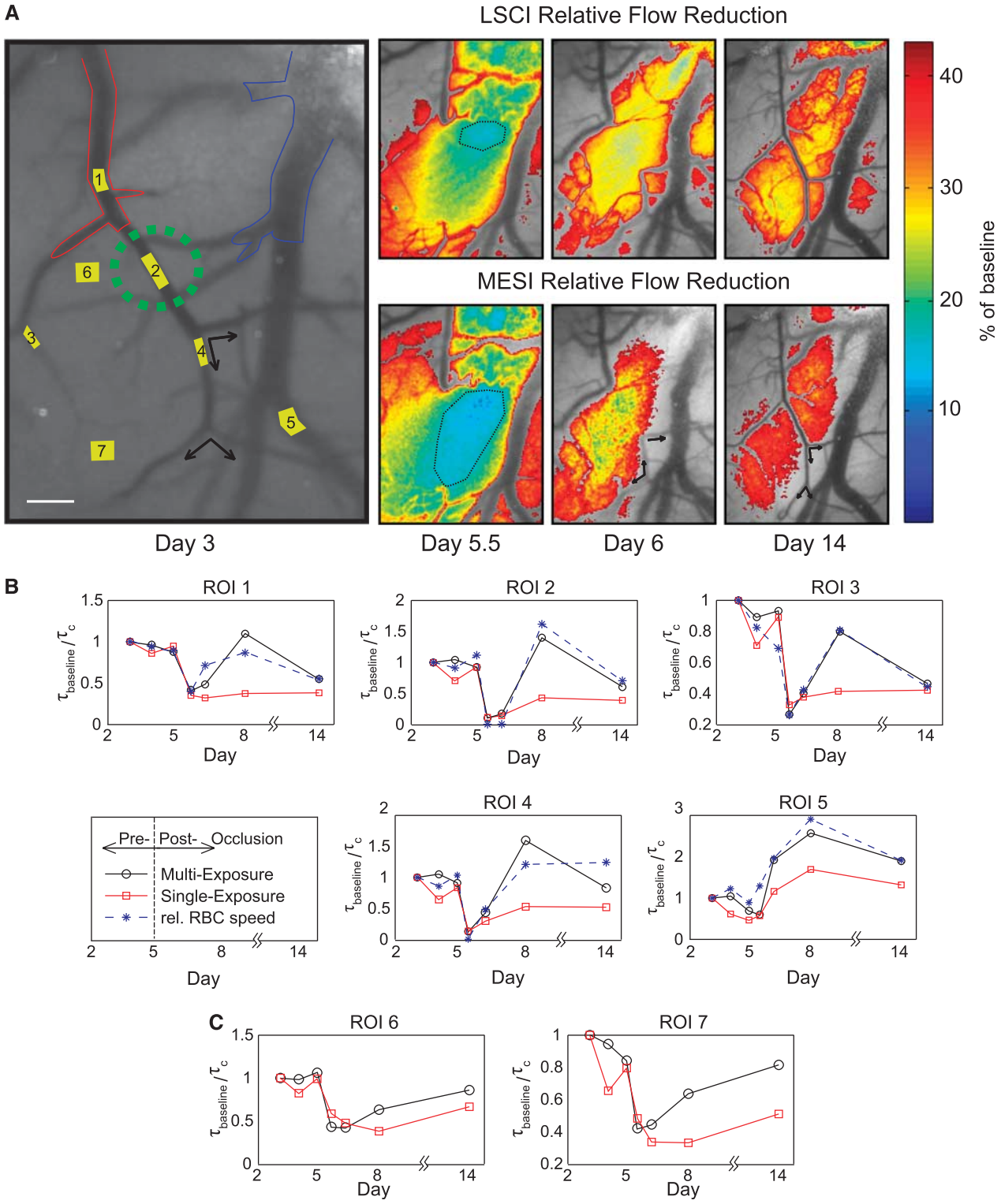

Figure 5. (**A**) Speckle contrast image sequence (5 ms exposure) of chronic flow dynamics. Day 3 speckle contrast image corresponds to baseline. Red outline identifies arteriole branch of the anterior cerebral artery and blue outlines highlights neighboring venule. Scale bar = 150 μm. Photo-thrombosis site is marked in green. Day 5.5 is the first imaging session after photo-thrombosis. Regional and magnitude variations between 5 ms exposure Laser Speckle Contrast Imaging (LSCI) (top row) and Multi-Exposure Speckle Imaging (MESI) flow predictions (bottom row) after occlusion are shown in overlay over the matching speckle contrast images with a 40% of baseline cutoff. Arrows indicate flow direction from red blood cell (RBC) tracking. Flow at 15% of baseline is demarcated by black outline on Day 5.5 and selections (white box) on Days 6 and 14 depict effect of illumination, sample orientation, and static scattering artifacts specifically on LSCI estimates versus MESI. (**B**) MESI and LSCI (5 ms) flow dynamics regions of interest (ROIs) over large microvasculature and (**C**) areas without obvious vasculature corresponding to ROI labels in (**A**).

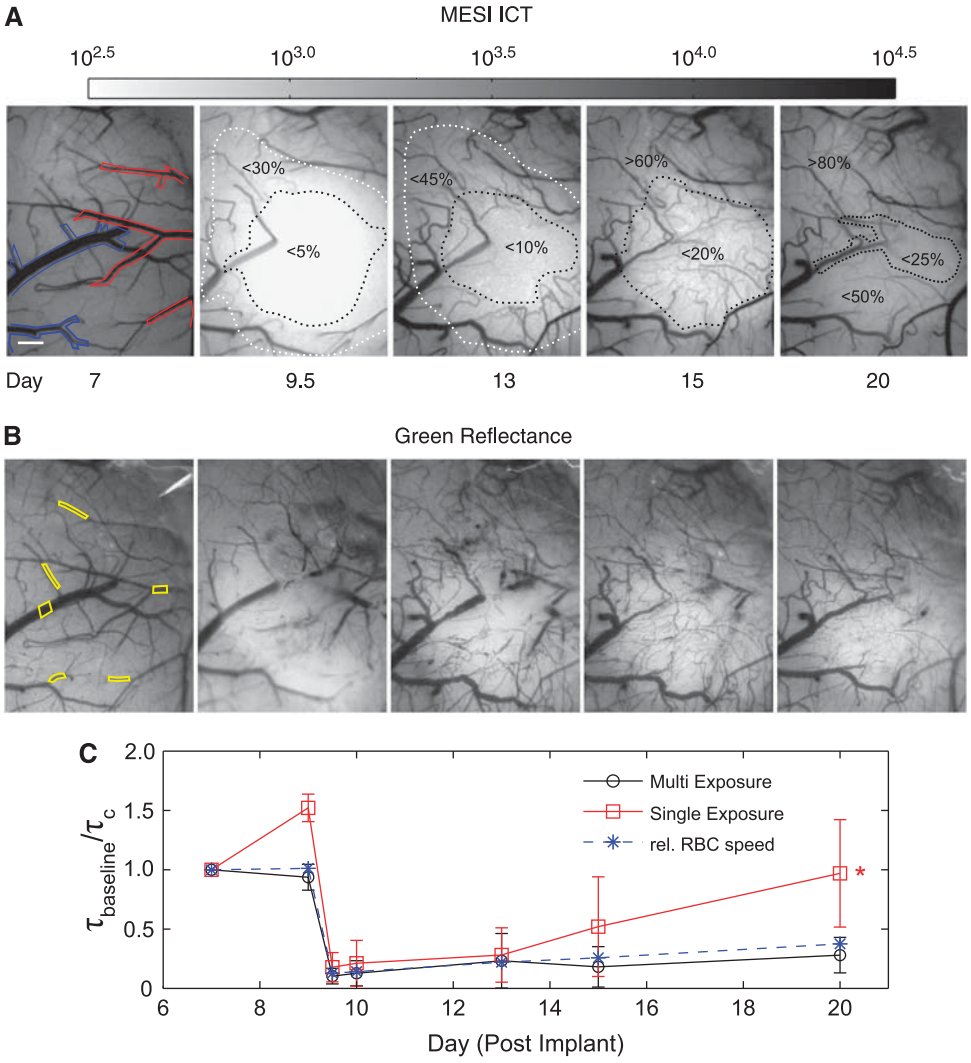

Figure 6. (**A**) Multi-Exposure Speckle Imaging inverse correlation time (MESI ICT) images of perfusion before and after photo-thromboses conducted between Days 9 and 9.5. Arteriole branches of the middle cerebral artery (MCA) are outlined in red and draining venules are outlined in blue in Day 7 baseline MESI image. Larger field of view (FOV) and logarithmic image scale is used to capture occlusion as well as residual flow, redistribution, and remodeling over the chronic period. Darker regions signify higher flow. Dashed outlines group flow dynamics according to percentage of baseline. Scale bar = 300 μm. (**B**) Corresponding green reflectance photography of the cortical surface. Labeled regions of interest (ROIs) correspond to both 5 ms exposure Laser Speckle Contrast Imaging (LSCI) and MESI computed flow indices averaged in (**C**). (**C**) Average flow dynamics from MESI and LSCI versus red blood cell (RBC) speed changes in six vessels. Flow measures are normalized to first imaging session. Asterisk denotes statistically significant (*$P < 0.05$, repeated measures analysis of variance) difference in flow predictions between LSCI (5 ms) and RBC tracking over all imaging sessions.

the MCA in another animal (Figure 6). The images offer a direct comparison between quantitative perfusion images obtained using MESI (Figure 6A) and green reflectance photography (Figure 6B) of the same region. Flow trends were followed nearly 2 weeks after occlusion over an expanded FOV (2.5 × 2 mm). By Day 13, there is a substantial flow redistribution surrounding a central reduction in flow of over 90% (Figure 6A). Chronic reflectance photographs (Figure 6B) help discern whether the residual and returning flows are within newly formed or shifted and flow-shunted existing microvasculature. Due to postocclusion stenoses, lumen sizes of large surface vasculature are best acquired from ICT images (Figure 6A). These images reveal the true cross-sections of flow versus reflectance photography, which may register trapped erythrocytes as part of vessel lumen and obscure moving RBCs as well. By Day 20, the targeted MCA branch does not reperfuse (Figure 6A) and its lumen is no longer discernable with entrapped erythrocytes (Figure 6B). Also, the preponderance of redistributed flows in superficial vessels appears reduced by Day 20 (Figures 6A and 6B) but regional perfusion levels increase to nearly 50% of baseline in what was a large section of the ischemic core. This may suggest a more mature vascular remodeling phase where flows are distributed through more underlying parenchymal microvasculature.

The RBC tracking was largely restricted to the flows in vessels beyond the ischemic core to clearly follow the selected vessels over the entire chronic period (Figures 6B and 6C). Laser Speckle Contrast Imaging ICTs suggest a significantly errant return to baseline levels in the selected ROIs by Day 20, along with significant baseline inaccuracies (Day 9, Figure 6C). On average, MESI estimates registered a nearly threefold lower percent deviation from RBC tracking ($\Delta = 10 \pm 5\%$) and higher

correlations ($r = 0.94 \pm 0.09$) than each of the three LSCI single exposures (Animal 9, Figure 3B).

DISCUSSION

Multi-Exposure Speckle Imaging as a Tool for Chronic Cerebral Blood Flow Imaging

The chronic studies (Figure 3B) consistently showed lower percent deviations between RBC speed dynamics and the ICTs computed using the MESI technique than those from the three common single exposures typically used for LSCI. Additionally, the paired ROIs over all animals yielded consistently higher correlation between RBC tracking and MESI. Within single exposures alone, some LSCI camera exposure durations (Figure 3B) better mirror the RBC flows than others due to better sampling of the inherent velocity distributions. However, the variability among animals as well as between imaging sessions and ROIs would suggest that no optimal choice of single-exposure duration exists to accurately map blood flow in all vessels, let alone after an induced flow change (Figures 4–6).

We have previously shown that MESI's quantitative accuracy and sensitivity are fairly robust over a large flow range.[23,24] The MESI model includes three decades of exposures including a decade longer than the single exposures selected for the current comparison. Longer exposures individually may be better for single-exposure imaging during prolonged periods of flow reduction. However, most longitudinal imaging studies will need to sample flow dynamics not only in the ischemic core but also in surrounding penumbra that include regions where flow may be shunted or redistributed and therefore necessitate the inclusion of shorter exposures. The ability to quantify varying regional flow dynamics accurately is one of the primary motivations for the multiexposure implementation.

The LSCI analysis is likely also affected by variations in the illumination over the FOV, the proportion of dynamic scattering, and instrument noise over the imaging sessions. The MESI speckle visibility expression (equation 2) attempts to account for these factors by mapping the dependence of the speckle contrast on the exposure duration while accounting for the mixing of static and dynamic scattering, exposure-independent noise, and the nonergodic nature of spatial contrast analysis of a temporal phenomenon (e.g., CBF). When baseline flow levels were relatively consistent (Figure 3), the sessions during which LSCI predictions significantly deviated from RBC tracking could be attributed to the variability in the orientation of the brain relative to the collection optics, intersession illumination variations, such as specular reflections, as well as an increase in dura mater or peripheral skull growth which would alter the static and dynamic scattering contributions in those regions. These factors contribute to the imaged speckles and further confound the flow contribution to the speckle contrast at the single exposures.

Studies using temporal processing of LSCI images[43,44] have shown improved flow sensitivity in the presence of static scatterers, such as skull. While these studies may appear to improve flow visibility, they have two significant limitations affecting flow quantification. One, temporally processed LSCI only partially addresses the problem of static scattering by only accounting for the nonergodic variance in equation (2), neglecting heterodyne mixing of static and dynamically scattered light, and two, the estimated blood flow measures are not more quantitative than spatially processed LSCI, as exhibited by the use of hybrid implementations.[44] Spatial analysis with heterodyne mixing models, such as MESI, allows for a more proper separation of statically and dynamically scattered light while better sampling the flow distributions by collecting significantly more information about the speckle decorrelation. This yields more quantitative estimates of blood flow consistently throughout the image. Additionally, the current MESI implementation with 15 exposures is overdetermined (equation 2), and an analysis of which and how few exposures are necessary will improve the technique's temporal resolution.

Ultimately, the chronic accuracy of the relative flow changes from speckle imaging was better attained by MESI's under 15% deviation with RBC tracking compared with under 40% for single-exposure LSCI (Figure 3B and 3C, $n = 9$ animals, $n = 201$ evaluation points). These bounds register the degree of confidence in the two speckle techniques to establish a quantitative baseline and therefore the ability to examine flow changes chronically. Particularly, these results suggest some potential for calibration within a single animal's cortical circulation to actual flows given the strong proportionality observed with the MESI technique. The degree to which cross-animal comparisons can be made quantitatively remains to be determined, as the spatially integrated light-tissue interactions being imaged may be highly dependent on the sample morphology, including the vascular architecture and hematocrit variations.

Furthermore, placing the spatially integrated speckle ICT measures directly to scrutiny against the absolute RBC velocity magnitudes would demand spatial decoupling and specificity of the dynamic light scattering technique, comprising an ill-posed inverse problem. To directly relate the scale of ICT with speed, one would require an active and independent calibration at each pixel of the speckle contrast image for each specimen. Nonetheless, administration of such analyses at some level was necessary to examine the relationship between ICTs from selected vessels with the RBC velocities. Neighboring and underlying flows may have an impact on the ICTs obtained from a single vessel ROI, which may result in substantial discrepancies if the adjacent flows are relatively large in magnitude. It is for this reason we restrained our cross-modality comparisons with planar and nonoverlapping vessel segments within the FOV.

Effects of Experimental Procedures

Some error between RBC tracking and the speckle imaging (MESI and LSCI) can be attributed to experiment protocol. Speckle imaging acquisition lasted 5 minutes as mentioned earlier. The RBC tracking was performed immediately thereafter, as the same camera was used for both imaging modalities. Slight excursions in animal heart rate of 20 to 30 b.p.m. out of 400 to 500 b.p.m., typical under inhalation anesthesia, were tolerated between speckle imaging and RBC tracking. These variations may alter the cardiac output, and subsequently CBF, consistency between the sequential imaging acquisitions on each day by $\sim 5\%$, assuming other rheological factors remain constant.

Dynamic Contrast: Scattering vs Absorption

The RBC reflectance imaging relies on intrinsic absorption contrast of the RBCs with blood plasma (Figure 6B), while the speckle techniques use dynamic scattering contrast. The interrogating wavelengths centered approximately at 520 nm for RBC tracking are selected within the range of hemoglobin absorption, whereas the 660-nm wavelength used for speckle imaging was selected beyond the main hemoglobin absorption range to maximize contrast contributions from scattering alone.

Though RBC tracking provides absolute velocities, there are notable constraints with (1) camera frame rate requirements, (2) limitations in magnification and FOV, and (3) observations of resolvable vasculature. If these constraints are not adhered to correctly, then velocity magnitudes can be significantly underestimated.[7] The MESI technique provides an adequate level of accuracy with the ability to also obtain regional perfusion information from unresolvable microvasculature within the parenchyma with fewer instrumentation constraints and tradeoffs, exhibited by the full FOV acquisitions. Some animal studies were excluded from this presentation due to the lack of

sufficient absorption contrast for RBC tracking from blood clots and hemorrhagic staining of the dural surface, even though the cranial windows retained sufficient dynamic scattering contrast for speckle imaging of the cortex. Increasing durations of chronic study may exacerbate this issue. Nonetheless, RBC reflectance tracking, if performed with sufficient spatio-temporal sampling and contrast, can register flow direction, thereby providing complementary information to speckle imaging when needed.

CONCLUSIONS

The blood flow measurements in the form of ICT maps obtained using the MESI technique are capable of highlighting regional perfusion boundaries within and surrounding ischemic infarcts. The MESI-computed flow measure can go beyond qualitative observations of vascular remodeling by providing a reliable spatial perfusion index to examine and help characterize patho-physiology. We assessed the CBF dynamics due to induced vascular occlusions in animals to determine the extent of the infarct, changes in flow distribution, and turnover of vasculature relative to an accurately estimated physiologic baseline. This comparison is now possible because of the increased quantitative accuracy of the MESI technique. Beyond observing baseline flows, the ability to quantitatively characterize postocclusion CBF dynamics via intrinsic optical flow measurements in a chronic setting provides a platform for assessing the efficacy of therapies aimed at flow restoration. The potential for examining the degree and latency of angiogenesis, collateral flow, vascular redundancy, and regional tissue perfusion from a scalable imaging technique allows MESI to be an apt tool for studying these dynamics and their possible roles in stroke recovery as well.

DISCLOSURE/CONFLICT OF INTEREST

The authors declare no conflict of interest.

REFERENCES

1 Dalkara T, Arsava EM. Can restoring incomplete microcirculatory reperfusion improve stroke outcome after thrombolysis? *J Cereb Blood Flow Metab* 2012; **32**: 2091–2099.
2 Font MA, Arboix A, Krupinski J. Angiogenesis, neurogenesis and neuroplasticity in ischemic stroke. *Curr Cardiol Rev* 2010; **6**: 238–244.
3 Murphy TH, Corbett D. Plasticity during stroke recovery: from synapse to behaviour. *Nat Rev Neurosci* 2009; **10**: 861–872.
4 Brown CE, Li P, Boyd JD, Delaney KR, Murphy TH. Extensive turnover of dendritic spines and vascular remodeling in cortical tissues recovering from stroke. *J. Neurosci* 2007; **27**: 4101–4109.
5 Roe AW. *Imaging the Brain with Optical Methods*. Springer: New York, NY, 2009.
6 Kleinfeld D, Mitra PP, Helmchen F, Denk W. Fluctuations and stimulus-induced changes in blood flow observed in individual capillaries in layers 2 through 4 of rat neocortex. *Proc Natl Acad Sci USA* 1998; **95**: 15741–15746.
7 Duncan DD, Lemaillet P, Ibrahim M, Nguyen QD, Hiller M, Ramella-Roman J. Absolute blood velocity measured with a modified fundus camera. *J Biomed Opt* 2010; **15**: 056014.
8 Ishikawa M, Sekizuka E, Shimizu K, Yamaguchi N, Kawase T. Measurement of RBC velocities in the rat pial arteries with an image-intensified high-speed video camera system. *Microvasc Res* 1998; **56**: 166–172.
9 Bonner R, Nossal R. Model for laser Doppler measurements of blood flow in tissue. *Appl Opt* 1981; **20**: 2097–2107.
10 Steinmeier R, Bondar I, Bauhuf C, Fahlbusch R. Laser Doppler Flowmetry mapping of cerebrocortical microflow: characteristics and limitations. *NeuroImage* 2002; **15**: 107–119.
11 Dunn AK, Bolay H, Moskowitz MA, Boas DA. Dynamic imaging of cerebral blood flow using laser speckle. *J Cereb Blood Flow Metab* 2001; **21**: 195–201.
12 Armitage GA, Todd KG, Shuaib A, Winship IR. Laser speckle contrast imaging of collateral blood flow during acute ischemic stroke. *J Cereb Blood Flow Metab* 2010; **30**: 1432–1436.
13 Ayata C, Dunn AK, Gursoy-Ozdemir Y, Huang Z, Boas DA, Moskowitz MA. Laser speckle flowmetry for the study of cerebrovascular physiology in normal and ischemic mouse cortex. *J Cereb Blood Flow Metab* 2004; **24**: 744–755.
14 Strong AJ, Bezzina EL, Anderson PJB, Boutelle MG, Hopwood SE, Dunn AK. Evaluation of laser speckle flowmetry for imaging cortical perfusion in experimental stroke studies: quantitation of perfusion and detection of peri-infarct depolarisations. *J Cereb Blood Flow Metab* 2005; **26**: 645–653.
15 Shin HK, Dunn AK, Jones PB, Boas DA, Moskowitz MA, Ayata C. Vasoconstrictive neurovascular coupling during focal ischemic depolarizations. *J Cereb Blood Flow Metab* 2005; **26**: 1018–1030.
16 Dunn AK, Devor A, Dale AM, Boas DA. Spatial extent of oxygen metabolism and hemodynamic changes during functional activation of the rat somatosensory cortex. *Neuroimage* 2005; **27**: 279–290.
17 Durduran T, Burnett MG, Yu G, Zhou C, Furuya D, Yodh AG *et al*. Spatiotemporal quantification of cerebral blood flow during functional activation in rat somatosensory cortex using laser-speckle flowmetry. *J Cereb Blood Flow Metab* 2004; **24**: 518–525.
18 Dunn AK, Devor A, Bolay H, Andermann ML, Moskowitz MA, Dale AM *et al*. Simultaneous imaging of total cerebral hemoglobin concentration, oxygenation, and blood flow during functional activation. *Opt Lett* 2003; **28**: 28–30.
19 Shin HK, Dunn AK, Jones PB, Boas DA, Lo EH, Moskowitz MA *et al*. Normobaric hyperoxia improves cerebral blood flow and oxygenation, and inhibits peri-infarct depolarizations in experimental focal ischaemia. *Brain* 2007; **130**: 1631–1642.
20 Zhang S, Murphy TH. Imaging the impact of cortical microcirculation on synaptic structure and sensory-evoked hemodynamic responses in vivo. *PLoS Biol* 2007; **5**: e119.
21 Strong AJ, Anderson PJ, Watts HR, Virley DJ, Lloyd A, Irving EA *et al*. Peri-infarct depolarizations lead to loss of perfusion in ischaemic gyrencephalic cerebral cortex. *Brain* 2007; **130**: 995–1008.
22 Duncan DD, Kirkpatrick SJ. Can laser speckle flowmetry be made a quantitative tool? *J Opt Soc Am A* 2008; **25**: 2088–2094.
23 Parthasarathy AB, Tom WJ, Gopal A, Zhang X, Dunn AK. Robust flow measurement with multi-exposure speckle imaging. *Opt Express* 2008; **16**: 1975–1989.
24 Parthasarathy AB, Kazmi SMS, Dunn AK. Quantitative imaging of ischemic stroke through thinned skull in mice with MultiExposure Speckle Imaging. *Biomed Opt Express* 2010; **1**: 246–259.
25 Tom WJ, Ponticorvo A, Dunn AK. Efficient processing of laser speckle contrast images. *IEEE Trans Med Imaging* 2008; **27**: 1728–1738.
26 Boas DA, Yodh AG. Spatially varying dynamical properties of turbid media probed with diffusing temporal light correlation. *J Opt Soc Am A* 1997; **14**: 192–215.
27 Wu X-L, Pine DJ, Chaikin PM, Huang JS, Weitz DA. Diffusing-wave spectroscopy in a shear flow. *J Opt Soc Am B* 1990; **7**: 15–20.
28 Pine DJ, Weitz DA, Chaikin PM, Herbolzheimer E. Diffusing wave spectroscopy. *Phys Rev Lett* 1988; **60**: 1134.
29 Dunn AK. Laser speckle contrast imaging of cerebral blood flow. *Ann Biomed Eng* 2012; **40**: 367–377.
30 Boas DA, Dunn AK. Laser speckle contrast imaging in biomedical optics. *J Biomed Opt* 2010; **15**: 011109.
31 Yuan S, Devor A, Boas DA, Dunn AK. Determination of optimal exposure time for imaging of blood flow changes with laser speckle contrast imaging. *Appl Opt* 2005; **44**: 1823–1830.
32 Bandyopadhyay R, Gittings AS, Suh SS, Dixon PK, Durian DJ. Speckle-visibility spectroscopy: a tool to study time-varying dynamics. *Rev Sci Instrum* 2005; **76**: 093110.
33 Drew PJ, Blinder P, Cauwenberghs G, Shih AY, Kleinfeld D. Rapid determination of particle velocity from space-time images using the Radon transform. *J Comput Neurosci* 2010; **29**: 5–11.
34 Wilson CA, Hatchell DL. Photodynamic retinal vascular thrombosis. Rate and duration of vascular occlusion. *Investig Ophthalmol Vis Sci* 1991; **32**: 2357–2365.
35 Watson BD, Dietrich WD, Busto R, Wachtel MS, Ginsberg MD. Induction of reproducible brain infarction by photochemically initiated thrombosis. *Ann Neurol* 1985; **17**: 497–504.
36 Domoki F, Zölei D, Oláh O, Tóth-Szűki V, Hopp B, Bari F *et al*. Evaluation of laser-speckle contrast image analysis techniques in the cortical microcirculation of piglets. *Microvasc Res* 2012; **83**: 311–317.
37 Rege A, Murari K, Seifert A, Pathak AP, Thakor NV. Multiexposure laser speckle contrast imaging of the angiogenic microenvironment. *J Biomed Opt* 2011; **16**: 056006.
38 Santisakultarm TP, Cornelius NR, Nishimura N, Schafer AI, Silver RT, Doerschuk PC *et al*. In vivo two-photon excited fluorescence microscopy reveals cardiac- and respiration-dependent pulsatile blood flow in cortical blood vessels in mice. *Am J Physiol Heart Circ Physiol* 2012; **302**: H1367–H1377.
39 Unekawa M, Tomita M, Tomita Y, Toriumi H, Miyaki K, Suzuki N. RBC velocities in single capillaries of mouse and rat brains are the same, despite 10-fold difference in body size. *Brain Res* 2010; **1320**: 69–73.
40 Shih AY, Driscoll JD, Drew PJ, Nishimura N, Schaffer CB, Kleinfeld D. Two-photon microscopy as a tool to study blood flow and neurovascular coupling in the rodent brain. *J Cereb Blood Flow Metab* 2012; **32**: 1277–1309.

41 Nishimura N, Rosidi NL, Iadecola C, Schaffer CB. Limitations of collateral flow after occlusion of a single cortical penetrating arteriole. *J Cereb Blood Flow Metab* 2010; **30**: 1914–1927.

42 Schaffer CB, Friedman B, Nishimura N, Schroeder LF, Tsai PS, Ebner FF *et al*. Two-photon imaging of cortical surface microvessels reveals a robust redistribution in blood flow after vascular occlusion. *PLoS Biol* 2006; **4**: e22.

43 Li P, Ni S, Zhang L, Zeng S, Luo Q. Imaging cerebral blood flow through the intact rat skull with temporal laser speckle imaging. *Opt Lett* 2006; **31**: 1824–1826.

44 Cheng H, Yan Y, Duong TQ. Temporal statistical analysis of laser speckleimages and its application to retinal blood-flowimaging. *Opt Express* 2008; **16**: 10214–10219.

Supplementary Information accompanies the paper on the Journal of Cerebral Blood Flow & Metabolism website (http://www.nature.com/jcbfm)